Mineralogy and Petrology (2022) 116:429–441
https://doi.org/10.1007/s00710-022-00794-y

ORIGINAL PAPER

Multi-stage alteration history of volcanic clasts containing buddigtonite from Upper Cretaceous strata of the Subsilesian Unit, Czech part of the Outer Flysch Carpathians

Dalibor Matýsek[1] · Petr Skupien[1] · Miroslav Bubík[2] · Jakub Jirásek[3] · Radek Škoda[4]

Received: 1 December 2021 / Accepted: 12 September 2022 / Published online: 10 October 2022

Abstract
Floods in 1997 and 2010 exposed the Frýdek and Frýdlant formations of the Subsilesian Unit in the Ostravice River bed near Frýdek-Místek. In the sedimentary sequence of upper Campanian to Maastrichtian marls and paraconglomerates, clasts of strongly altered basic volcanic rock were found, accompanied by carbonate concretions and layers. Rare apatite, biotite, and a Cr-rich spinel subgroup mineral are the only relatively well-preserved primary minerals in the clasts. The matrix contains buddingtonite, albite, sanidine, kaolinite, illite-muscovite, a mineral of the smectite group, and possibly also a mixed structure mineral of the chlorite-smectite type. Laths of buddingtonite, identified by powder X-ray diffraction and wavelength-dispersive X-ray spectrometry, are not homogenous. Their compositions range from Bd_{41} to Bd_{59} molar component, with Kfs ranging between 26 and 35 mol%, Nafs between 5 and 27 mol%, and Ca-feldspar between 1 and 4 mol%. The matrix is irregularly dolomitized. Carbonates are also present in pseudomorphs after idiomorphic olivine and in fill of amygdaloidal cavities. These carbonates reveal complicated alteration rock history, having cores of magnesite passing into almost pure siderite outer parts. Calcite is always the youngest and most homogenous carbonate, probably connected with a different geological event. Accompanying carbonate concretions are composed of three dolomitic phases with quartz, calcite, and muscovite. We can conclude that buddingtonite originates in alteration of primary feldspar and/or volcanic glass during the catagenetic breakdown of kerogen in the sediment, surrounded by clayey sediments rich in decomposing organic matter. Volcanic clasts have similar texture and supposed pre-alteration phase composition as the rocks of teschenite association, namely monchiquites to picrites. However, the source of volcanic clast within the sediments remains unclear.

Keywords Buddingtonite · Powder X-ray diffraction · Volcanic rock · Cretaceous · Western Carpathians

Introduction

Buddingtonite is an ammonium analog of potassium feldspar. It was described in 1964 from strongly hydrothermally altered andesites (Erd et al. 1964). In the original description, it contains zeolite water in the amount of about 0.5 apfu. The authors state that it is a biaxial, monoclinic, space group $P2_1$ or $P2_1/m$. According to Erd et al. (1964), buddingtonite was formed by the transformation of plagioclase of medium basicity in the environment of a hot mineral water spring containing 460–540 ppm NH_3 associated with volcanism. Subsequently, it was verified on the holotype material that buddingtonite is anhydrous and the previously determined water content comes from an admixture of montmorillonite clay mineral (Voncken et al. 1993). Hydrothermal buddingtonite of similar genesis was also described by Pampeyan (2010).

Editorial handling: N. V. Chukanov

✉ Jakub Jirásek
jakub.jirasek@upol.cz

[1] VŠB - Technical University of Ostrava, Faculty of Mining and Geology, Department of Geological Engineering, 17. listopadu 15/2172, 708 33 Ostrava, Poruba, Czech Republic

[2] Czech Geological Survey, Leitnerova 22, 658 69 Brno, Czech Republic

[3] Jakub Jirásek, Faculty of Science, Department of Geology, Palacký University Olomouc, 17. listopadu 1192/12, 771 46 Olomouc, Czech Republic

[4] Masaryk University, Faculty of Science, Department of Geological Sciences, Kotlářská 267/2, 611 37 Brno, Czech Republic

More important and also more interesting from the sedimentological point of view are the findings of authigenic buddingtonite or transient members of the buddingtonite – K-feldspar series in sedimentary sequences. It is evident that under certain conditions, buddingtonite may form in sediments during diagenesis, either by direct crystallization or more likely by a transformation from other feldspars. The first findings on probably diagenetic buddingtonite were reported by Gulbrandsen (1974) from the Phosphoria Formation from SE Idaho, USA. This author stated that buddingtonitic feldspar (most often between $Bd_{72}KF_{28}$ to $Bd_{50}KF_{50}$) is abundant, sometimes up to 50 vol% component of mudstone, which also contains albite, illite and minor amounts of montmorillonite, dolomite, phosphorite, and silicite. Gulbrandsen (1974) assumed that buddingtonite was formed by alteration of volcanic glass in an environment with a high content of ammonium ions. Diagenetic buddingtonite was described from oil shales of Queensland, Australia, by Loughnan et al. (1983). In a similar geological setting, the phase was reported by Oh et al. (1993) from the Green River Formation, Colorado, USA. Authigenic buddingtonite from sandstones was described by Ramseyer et al. (1993). Based on results of isotope analyzes, these authors stated that NH_4-K feldspar was formed in the methanogenetic zone at 28 °C (that is, early diagenetic) in an anoxic environment, and that NH_4 for buddingtonite formation originated from the initial phase of organic matter destruction. The mineral was also found in coal with extremely high sulfur content, where it was probably formed by transformation, i.e. ion substitution from clastic potassium feldspar (Dai et al. 2018).

The crystallographic properties of synthetic as well as deuterated buddingtonite were discussed by Harlov et al. (2001) and Mookherjee et al. (2004). Powder neutron diffraction data indicate that it is isostructural with sanidine. The mineral is monoclinic with topochemical symmetry C2/m, which corresponds to high sanidine, i.e. sanidine with a high degree of Si/Al disorder in tetrahedral positions, and the lattice parameters (at 280 K) are a = 8.8301 Å, b = 13.075 Å, c = 7.1957 Å, β = 116.7° (Mookherjee et al. 2004). Compared to K-feldspars, buddingtonite shows a significant expansion of the parameter a (by about 0.2 Å) and also the unit cell volume (by about 20 $Å^3$), which is related to certain differences in the ionic radii NH_4^+ and K^+ (Harlov et al. 2001). Pöter et al. (2007) reported a very close dependence of the NH_4/K isomorphic substitution on the lattice parameters of synthetic buddingtonite, which can also be used quantitatively. Pöter (2003, 2007) further states that under metamorphic conditions (600 °C, 400 MPa) and high concentrations of NH_4^+, NH_4-feldspar is not formed, but rather a mica mineral of the muscovite-tobelite series. The synthesis of buddingtonite under hydrothermal conditions is reported by Voncken et al. (1988) at temperature 550–600 °C and pressure 2 kbar.

The aim of the present contribution is the first description of buddingtonite and its geological setting from the Carpathian Mountains. This mineral was discovered during the study of temporarily exposed sediments of the Outer (Flysch) Carpathians in the Ostravice riverbed, north of Frýdek-Místek, Czech Republic (Fig. 1). Buddingtonite was found to be a microscopic component of extremely strongly altered clasts of basic igneous rocks of unclear provenance, perhaps monchiquites to picrites, which are closely associated with concretions of dolomite carbonates.

Geological setting

The Outer Flysch Carpathians represent the most external zone of the Carpathian mountain chain, part of the Alpine-Carpathian-Dinaridic orogenic system. They comprise a structurally complex area that consists of folded and thrusted strata of the latest Jurassic to Lower Miocene age. In their present form, the Outer Flysch Carpathians consist of two groups of nappes (Fig. 1a): the Outer Group of Nappes (divided from lowest to highest into the Pouzdřany, Ždánice-Subsilesian,Silesian and Foremagura nappes/units) and the Magura Group of Nappes (divided into the Rača, Bystrica, and Bílé Karpaty nappes/units). The whole nappe allochthon is thrusted more than 60 km over the Miocene sediments of the Carpathian Foredeep (Picha et al. 2006).

The Subsilesian Nappe consists of Upper Cretaceous to Lower Miocene hemipelagic and flysch sediments deposited in the Silesian Basin (Menčík et al. 1983; Picha et al. 2006). They represent marine sediments of the continental slope and ridge. Four lithostratigraphic units were defined here, from the oldest: Frýdek, Frýdlant, Menilite, and Ženklava formations (Eliáš 1998; Bubík et al. 2016).

Floods in 1997 and especially in 2010 exposed extensive outcrops of the Subsilesian Unit in the Ostravice riverbed north from Frýdek-Místek, between villages Lískovec and Žabeň. The outcrops extends from GPS (Global Positioning System) coordinates N 49°42.65'; E 18°19.15' to N 49°41.83'; E 18°19.62'. They were mostly temporary, today it is possible to observe only its isolated parts, especially along the streamline of the river. The reason is both the instability of rocks (swelling, wilting), caused by the admixture of swellable clay minerals, as well as covering of the outcrops by fluvial gravel and vegetation. The outcrops were exposed due to the progressive deepening of the river erosive base, possibly more than 4 m.

Based on micropaleontological data and lithology, the outcrops represent tectonic slices of the Frýdek Formation (Campanian–Maastrichtian gray to brown-gray siltstones

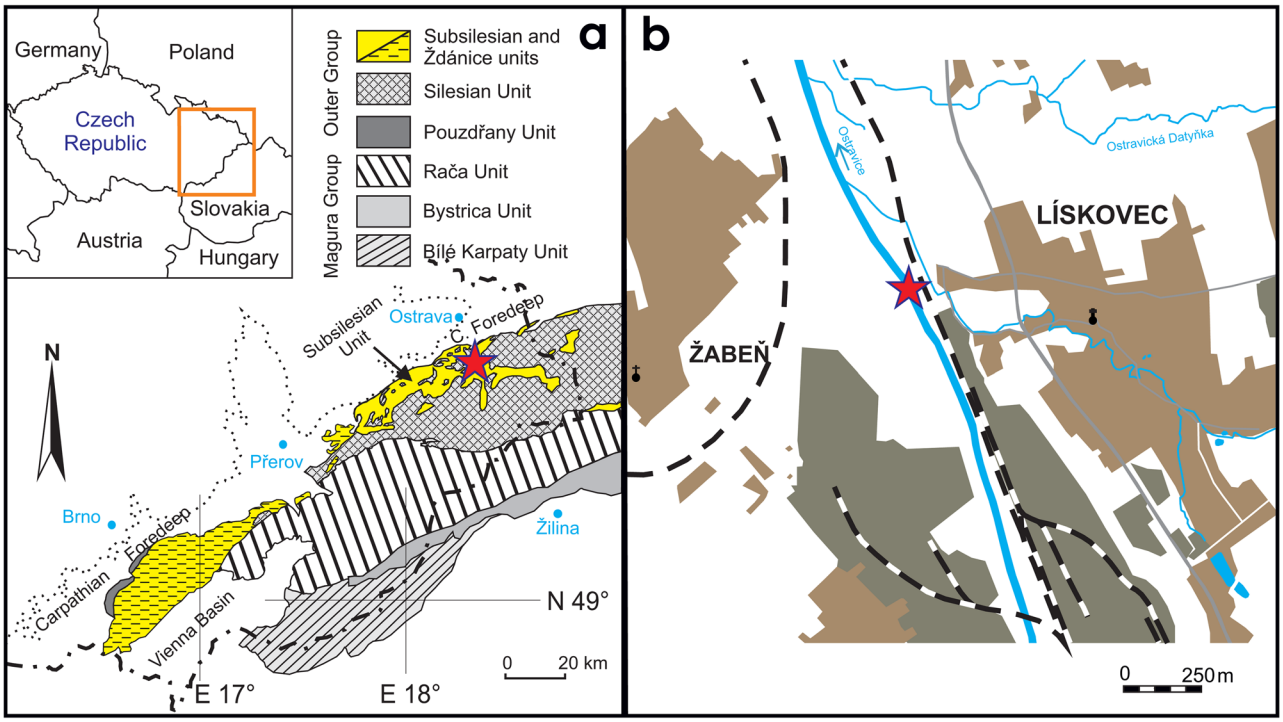

Fig. 1 Location of the investigated samples. **a** tectonic map of the Outer Western Carpathian area of the Czech Republic (after Menčík et al. 1983 and Picha et al. 2006, modified), **b** location map for Lískovec-Žabeň section

with bodies of pebbly mudstones and turbidite sandstones-conglomerates), the Frýdlant Formation (uppermost Paleocene variegated clay and Eocene mottled gray-green clay) and Krosno Formation (lowermost Miocene thin- to medium-bedded turbidites; see Fig. 2). Prevailing lithology is typical for Upper Cretaceous-Paleogene strata of the Subsilesian Unit described by previous authors (Eliáš 1998; Menčík et al. 1983).

The Menilite Formation is mostly missing in the section due tectonic reduction, except thin tectonic slice of lowermost Oligocene black-brown mudstone (Subchert Member?). Most of the pelitic rocks are affected by strong to extreme tectonic reworking (cleavage, wrinkling, and local mylonitization). Clasts of igneous rock with buddingtonite were found on the left bank of the Ostravice River, about 50 m north of the effluent from the wastewater treatment plant, GPS coordinates N 49° 42.35'; E 18° 19.39'.

The strata at the locality are overturned as evident from gradation and sequence of turbidite intervals in sandstones and conglomerates. They may be assigned to the Frýdek Formation. A stratigraphical sequence comprises (from base to top and from south to north): (i) 5 m thick dark gray silty claystone with intercalations of poorly cemented sandstones and rare pebbles. Downward continuation of the claystone is covered by fluvial gravel. (ii) 14 m thick sequence of sandstones and conglomerates. The basal part of the sequence comprise oligomictic conglomerate passing with positive gradation to pebbly sandstone, and higher, laminated silty sandstone with coalified phytodetrite admixture. Top of the sequence consists of the conglomerate with 1,8 m thick submarine slump layer of poorly sorted sandstone enclosing clasts of basic volcanic rocks and large gray carbonate concretions. Planktonic foraminifers *Laeviheterohelix glabrans* (C.), *Ventilabrella* cf. *acervulinoides* (E.) and *Globotruncanella petaloidea* (G.) from lens of brown grey mudstone indicate Maastrichtian(?) age. (iii) 16 m thick pebbly mudstone (paraconglomerate). A matrix consists of brown-gray to gray calcareous mudstone to sandy siltstone and enclose quartz pebbles and 10 to 30 cm (max. 90 cm) clasts of various rocks, mostly limestones. The matrix highly prevails over the clasts. The large clasts are dominated by dark-gray limestones (Devonian-Mississippian) and light beige Štramberk-type limestone (Tithonian-Berriasian). Non-calcareous dinoflagellates *Areoligera senonensis, Cerodinium diebelii, C. speciosum, Isabelidinium cooksoniae, Leberidocysta chlamydata* from the matrix point to the late Campanian-early Maastrichtian. Planktonic foraminifers *Laeviheterohelix glabrans* (C.), *Rugoglobigerina pennyi* Br. and *Globotruncanella petaloidea* (G.) give evidence of late Campanian–Maastrichtian age.

The clasts of altered basic igneous rocks can be macroscopically described as easily disintegrating light gray-green, rusty weathered volcanite. The largest one found was ca. 65×30 cm and showed zoning in grain size. The outer part was clearly

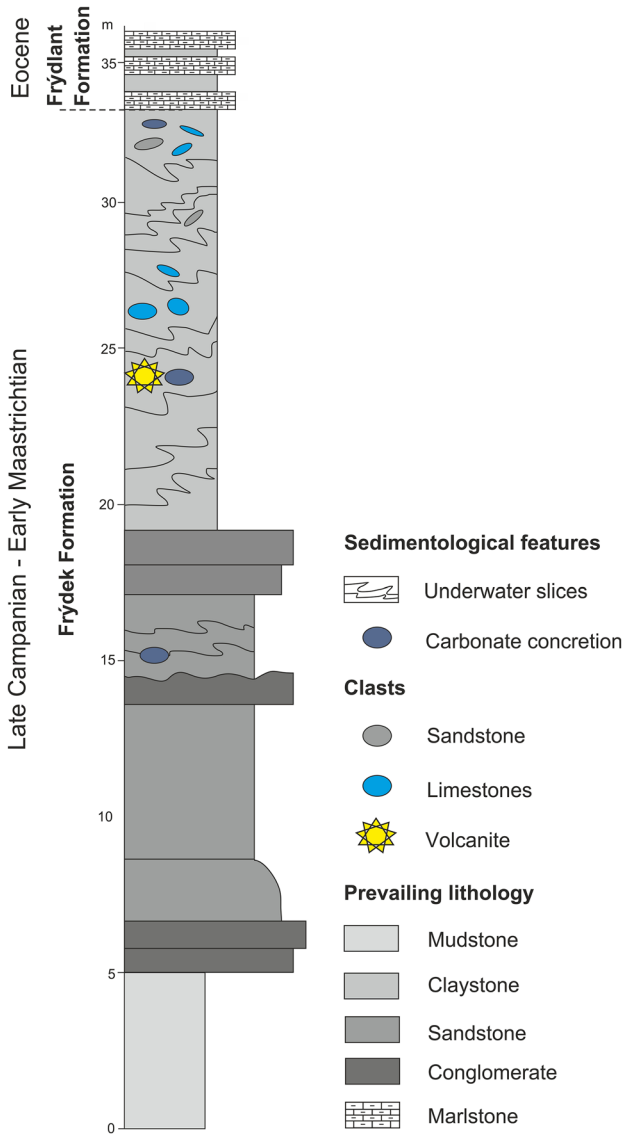

Fig. 2 Lithological log of the Lískovec/Žabeň section

more homogeneous and fine-grained than the central. It cannot be ruled out that this might be actually a volcanic bomb with an originally glassy surface. This boulder was associated with two concretions of dolomite carbonates.

Methods

Samples of basic igneous rock clasts, carbonate concretions, and surrounding aleuropelites were studied using powder X-ray diffraction (PXRD) analysis, a field emission scanning electron microscope (FESEM) equipped with energy-dispersive X-ray spectrometer (EDS) and back-scattered electron detector (BSE), and an electron probe micro-analyser (EPMA) with wavelength-dispersive spectrometers (WDS). Classical optical microscopy in transmitted light did not yield reliable results due to alterations and the associated opacification of minerals.

Powder X-ray diffraction analyses were carried out using a Bruker-AXS D8 Advance instrument with a 2θ/θ measurement geometry and position-sensitive detector LynxEye under the following conditions: Cu-Kα radiation (Ni filter), voltage 40 kV, beam current 40 mA, step mode with a step size of 0.014° 2θ, 0.25 s per step, and summation of five measurements. Qualitative analysis of diffraction patterns was performed using the EVA software (Bruker-AXS) and the database PDF-2, release 2011 (International Centre for Diffraction Data). The Rietveld method using the TOPAS software, version 5 (Bruker) was applied to verify the qualitative analyses and to quantify the mineral phases present. Input structural data for buddingtonite are adapted from Mookherjee et al. (2004). Unit cell parameters were refined by Le Bail full profile fitting too.

Microscopic investigation and EDS microanalysis were carried out on an electron microscope FEI Quanta 650 FEG. Analyses were made using both polished thin sections and natural fracture surfaces that were coated with a 35 nm thin film of Cr under the following conditions: 15 kV beam voltage, 8–10 nA current, 5–6 µm beam diameter, and a vacuum $< 10^{-3}$ Pa. Identification and quantification of spectral lines was performed using the decomposition method employing halographic peak deconvolution. Photomicrographs were taken with a BSE detector operated in chemical gradient mode.

Chemical composition of buddingtonite and carbonates were studied with an EPMA Cameca SX 100. The following conditions were used: WDS, accelerating voltage 10 keV (15 keV for carbonates), beam current 10 nA, beam diameter 8 µm. The following well defined natural minerals and synthetic phases were used for calibration: BN (N-Kα), albite, (Na-Kα), sanidine (Si-Kα, Al-Kα, K-Kα), wollastonite (Ca-Kα), $SrSO_4$ (Sr-Lα), and baryte (Ba-Lα) for buddingtonite analyses, and Mg_2SiO_4 (Mg-Kα), wollastonite (Si-Kα), $SrSO_4$ (Sr-Lα), baryte (Ba-Lα), vanadinite (Pb-Mα), fluorapatite (Ca-Kα), sanidine (K-Kα), hematite (Fe-Kα), Mn_2SiO_4 (Mn-Kα), Co metal (Co-Kα), gahnite (Zn-Kα) and topaz (F-Kα) for carbonate analyses.

Special care was taken in determining N in feldspars. Nitrogen was measured using a 60 Å W/Si pseudo-crystal monochromator in an integrated peak-area mode at the beginning of the analysis at mild analytical conditions (accelerating voltage of 10 kV, beam current of 10 nA and 8 µm electron beam diameter) to avoid any electron beam-induced sample decomposition. Further increase of the diameter of the analytical spot was impractical, because of the small sizes of crystals to be analysed. The N-Kα line was measured and BN was used for calibration. As N concentrations in calibrant

material and unknowns differed appreciably, background correction was done using the background of N-free microcline. At the mild conditions used and 180 s counting time, the detection limit for N based on counting statistics was ~ 0.7 wt%. The estimated standard deviation for a concentration of 3 wt% N concentration was ~ 18%. The measured intensities were processed for matrix effects using X-PHI correction routine (Merlet 1994).

Microfossils from pelitic rocks were extracted using standard micropaleontological methods. Samples for foraminifers were disintegrated in hot solution of sodium carbonate and washed on the sieve 0.063 mm. Samples for non-calcareous dinoflagellates were treated with HCl to remove the calcareous fraction and with HF to remove silicates. Sieving was performed using a 15 µm nylon mesh. Oxidation was not used.

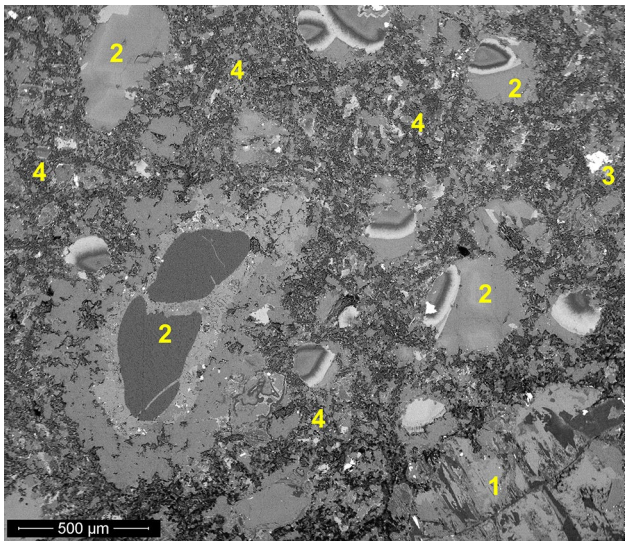

Fig. 3 FESEM-BSE images documenting the polyphase alteration of basic volcanic rock. 1 – carbonatised olivine phenocryst, 2 – amygdales filled by various carbonates, 3 – anatase pseudomorph after Ti-bearing magnetite, 4 – smectitized, kaolinized, dolomitized, and feldpsathitized matrix

Results

The results of powder X-ray diffraction and electron microanalyses show that the *clasts of the basic volcanic rock* from the locality represent an example of the extreme alteration in a sedimentary environment. The only relatively well-preserved primary minerals are quite rare and very small crystals of *accessories*–apatite, biotite, and very rare Cr-rich spinel subgroup member. Polyphase carbonatization, transformation to clay minerals, and alteration of feldspars with the formation of buddingtonite and albite can be observed microscopically (Fig. 3).

Apart from the above-mentioned pseudomorphs, *carbonates* are also present as fillings of amygdales and locally carbonatized rock matrix. Diffraction patterns close to dolomite and the siderite–magnesite series dominate, while calcite is contained only in small amounts. The diffraction lines of the carbonates are asymmetric, inhomogeneous to split. The results of modeling using the Rietveld method show the presence of two to three carbonates from the siderite-magnesite series and three phases from the dolomite group: Fe-(Ca)-rich dolomite, Fe-rich dolomite, and dolomite. Carbonate phases differ slightly in lattice parameters, but those in carbonates cannot be reliably interpreted concerning their chemistry only based on X-ray diffraction results. However, the presence of members, i.e. siderite, magnesite, and dolomite, is indisputable.

The presence of *buddingtonitic feldspar* in the studied samples is manifested compared to potassium feldspar not only by a clear shift of diffraction lines but also by an atypical course of their intensities. In buddingtonite, some diffraction lines are strongly overestimated in intensity, while others show decreased values. This is due to significant differences in the linear absorption coefficients of the ("extra framework") K^+ and NH_4^+ ions. The increase in line intensities from areas (020) and (-201) and a slight decrease in intensities at lines (-112), (131) are particularly marked. Lines (130), (002), and (-202) are without significant changes.

Unit cell parameters are given in Table 1, with the statistical parameters of the Rietveld refinement as follows: Rexp: 1.76, Rwp: 2.80, Rp: 2.15, GOF (goodness-of-fit): 1.59. The interpreted powder X-ray diffraction pattern is available in the ESM (Electronic supplementary material). The parameter "a" from both calculation methods indiicates, based on the dependencies on the proportion of NH_4^+ (Pöter et al. 2007), up to about 60 mol% of buddingtonite component. The dependencies for other unit cell parameters are not very significant in this respect.

Results of WDS microanalyses of buddingtonitic feldspar are given in Table 2. It can be seen that the content of the budingtonite component is in the range between 44 and 59 mol% and NH_4^+ is in all cases the predominant component in the A structure position. Other cations at the A position include K (0.26–0.35 apfu) dominating over Na (0.05–0.27 apfu) and Ca (0.01–0.04 apfu). The analysis results of spot number 5 with an elevated Na content are perhaps affected by the presence of microinclusions of Na feldspar or by local albitization of the sample. BSE images very often show some inhomogeneities in buddingtonite (Fig. 4b).

In addition to buddingtonite, the samples also contain small amounts of albite, a possible admixture of Na-rich sanidine.

Table 1 Unit-cell parameters of buddingtonite, in comparison with published data (including monoclinic K-feldspars: sanidine and orthoclase)

Data source	Sample	Method	a (Å)	b (Å)	c (Å)	β (°)
Present study	Natural buddingtonite	Rietveld refinement	8.7364 – 8.7436	13.0117 – 13.0243	7.1887 – 7.1981	116.025 – 116.084
		Le Bail refinement	8.742 – 8.746	13.017 – 13.021	7.190 – 7.197	115.968 – 16.083
Erd et al. (1964)	Natural buddingtonite - holotype	Calculated from the diffraction positions, $P2_1$ $P2_1/m$	8.571	13.032	7.187	112.733
Kimball and Megaw (1974)	Natural buddingtonite - holotype	Calculated from the diffraction positions, C2/*m*	8.804(2)	13.024(3)	7.183(1)	116.105(18)
Venari et al. (2017)	Natural buddingtonite	Rietveld refinement	8.805(1)	13.043(1)	7.200(1)	116.107(7)
Voncken et al. (1988)	Buddingtonite synthetized at 550–600 °C and 2 kbar	Calculated from the diffraction positions	8.824(5)	13.077(8)	7.186(4)	116.068(12)
Mookherjee et al. (2004)	Buddingtonite synthetized at 600 °C and 500 MPa	Rietveld refinement	8.83157	13.08541	7.20024	116.147
Harlov et al. (2001)	Buddingtonite synthetized at 400–500 °C and 500 MPa	Rietveld refinement	8.8251 –8.8398	13,0411 – 13.0641	7,1875 – 7,1935	116,108 – 116,285
Pöter et al. (2007)	Buddingtonite synthetized at 400–500 °C and 400–500 MPa	Rietveld refinement	8.8254 – 8.8408	13.0423 – 13.0630	7.1867 – 7.1938	116.110 – 116.289
Angel et al. (2013)	Sanidine	Single-crystal diffraction	8.5497	13.0216	7.1843	115.988
Angel et al. (2013)	Orthoclase	Single-crystal diffraction	8.5739	12.9874	7.2018	116.042

Kaolinite, illite-muscovite, a mineral of the smectite group, and possibly a mixed structure mineral of the chlorite-smectite type were found among present clay minerals by PXRD (see ESM). Illite-muscovite, anatase, and apatite were found as accessories.

The presence of smectite, or a mineral with a mixed-layer structure of the chlorite-smectite type, is manifested by a wide diffraction band with an interlayer distance of about 14.5 Å. After the application of ethylene glycol, there is a slight expansion to 16.8 Å. The mineral shows a low degree of crystallinity. Superstructural diffraction maxima corresponding to an ordered mixed corrensite-type structure were not found.

Our FESEM-BSE images obtained from polished sections indicate practically total destruction of the primary volcanic mineral components, and also wide inhomogeneity of the matrix in particular (Fig. 4a). Pseudomorphs after hypidiomorphic olivine, composed of dolomite, with siderite edges, and around the original cracks, are relatively rare. Locally, quartz is present in the form of thin veins around pseudomorph cracks. Other mafic minerals do not form well-developed pseudomorphs and are replaced by mixed-layer chlorite-smectite structures. Kaolinite is probably the youngest phase; it is present in fine-grained to powdery aggregates that fill irregular polygonal spaces, possible pseudomorphs after analcime.

The matrix is very fine-grained and locally completely dolomitized. Irregular dolomite grains contain numerous inclusions. Outside these dolomitized areas, the matrix consists of very small, densely crowded, and imperfectly crystallized tabular crystals of predominantly feldspar composition (Fig. 4a, b). It is evident in the BSE images that the feldspar aggregates are highly inhomogeneous (Fig. 4b). Overall, they show low reflectivity but contain lighter domains. EDS microanalyses show that the darker regions contain, in addition to Si and Al (ratio ca. 3:1), also smaller amounts of K and qualitatively detectable nitrogen. Atomic K/Al ratios tend to be less than 0.5. The composition of the dark areas, therefore, corresponds to feldspar of the buddingtonite-potassium feldspar series. The lighter areas contain Na admixture and probably less nitrogen. In the feldspar mass, extremely small apatite particles and dark mica tables are present.

Table 2 Chemical compositions and calculated mineral formulae of buddingtonitic feldspar

Analysis	Mean	1	2	3	4	5	6
Major oxides (wt%)							
SiO_2	66.73	67.13	66.92	66.44	66.69	66.36	66.86
Al_2O_3	19.56	19.27	19.86	19.31	19.35	19.72	19.85
CaO	0.43	0.18	0.32	0.28	0.51	0.84	0.10
Na_2O	1.52	0.63	1.37	1.18	3.11	2.19	0.66
K_2O	5.47	5.69	5.89	6.10	4.56	4.81	5.78
$(NH_4)_2O$	5.12	5.42	5.20	5.05	4.28	5.13	5.64
Total	98.76	98.32	99.56	98.36	98.50	99.05	98.89
Calculated mineral formulae (apfu)*							
Si^{4+}	2.973	2.989	2.963	2.979	2.981	2.962	2.963
Al^{3+}	1.027	1.011	1.037	1.021	1.019	1.038	1.037
T site	4.000	4.000	4.000	4.000	4.000	4.000	4.000
Ca^{2+}	0.019	0.009	0.015	0.013	0.024	0.040	0.010
Na^+	0.132	0.054	0.118	0.103	0.270	0.190	0.057
K^+	0.311	0.323	0.333	0.349	0.260	0.274	0.327
NH_4^+	0.526	0.557	0.531	0.523	0.441	0.528	0.577
A site	0.988	0.943	0.997	0.988	0.995	1.032	0.971

Ba and Sr were always below the detection limits

*Calculated based on 4 (Si + Al) atoms in the tetrahedral sites

Cr-rich spinel subgroup mineral grains, small but quite abundant mineral particles from the TiO_2 group (probably anatase in pseudomorphs after Ti–rich magnetite), pyrite grains, exceptional sphalerite, and grains consisting of Ni–Fe-Co sulfide (pentlandite?) and Ni sulfide (millerite?) have been identified as very rare accessories. Ni-containing sulfides occur in pseudomorphs after olivine.

An interesting component of the studied altered basic volcanic clasts, observable especially in FESEM-BSE, are carbonates of amygdale fillings (Fig. 4c and in detail in Fig. 4e, f) and also in some pseudomorphs after olivine (Fig. 4d). These amygdales are oval or even variously deformed and are not always contrast-restricted to the surroundings (Fig. 4c). Diffusion transitions from almost pure magnesite to almost pure siderite can very often be observed in these cavities (Fig. 4e, f). Magnesite-siderite mixed crystals are sometimes idiomorphic, while the magnesite part of the crystal is the oldest and in contact with amygdale wall. The transition to siderite is usually asymmetric within a single crystal. Figure 5 shows distribution maps of one of the characteristic polycomponent carbonate fillings. It is clear that the substitution of Mg after Fe has a decisive influence on the resulting chemistry. Amygdales filled with the dolomitic phase are also very abundant. The microscopic character of the carbonate transition is also interesting, but difficult to interpret–at the interface between magnesite and Mg-rich siderite it is possible to observe signs of a fibrous structure. It could be a result of diffusion and replacement in a solid state. The usual concentric zoning is rarely developed and insignificant.

Calcite was detected by FESEM-BSE only as a filling of hairline cracks in both altered basic volcanitc rocks and surrounding carbonate concretions and sediments. Two generations of calcite in cracks of carbonates differ in Fe content. Similar calcite veins are quite abundant at the locality and it is probably a manifestation of syn- or post-tectonic, low-thermal hydrothermal activity connected to the Subsilesian Unit development, while calcite is clearly younger than mineral paragenesis of the altered volcanic clasts.

The chemical composition of carbonates of the studied basic volcanic clasts was studied using FESEM-EDS as well as by means of EPMA-WDS microanalyses (Table 3). The results are shown in the triangular classification diagram of Ca-Mg-Fe (Fig. 6). The fraction of Mn in the studied carbonates is very low, near the EDS detection limit (according to WDS up to 0.5 wt% MnO). Figure 6 shows that there is a continuous transition from magnesite to siderite. It is also evident that a slight trend from siderite to dolomite is indicated, consisting in an increase in Ca in siderite and siderite with a slightly increased Mg content. The amount of Pb, Ba, and Sr was always below the detection limits.

The dominant component of the *carbonate concretions* in the vicinity of the volcanic clasts is dolomite, which is also evidently diffractively inhomogeneous. Its diffraction lines are also clearly asymmetric towards lower angles (Fig. 7). According to Rietveld's analysis, it most likely consists of three close dolomitic phases (Fig. 7). Most likely, dolomite, dolomite with a slightly increased Fe content, and possibly also a dolomitic phase with an excess of Ca, i.e. the so-called

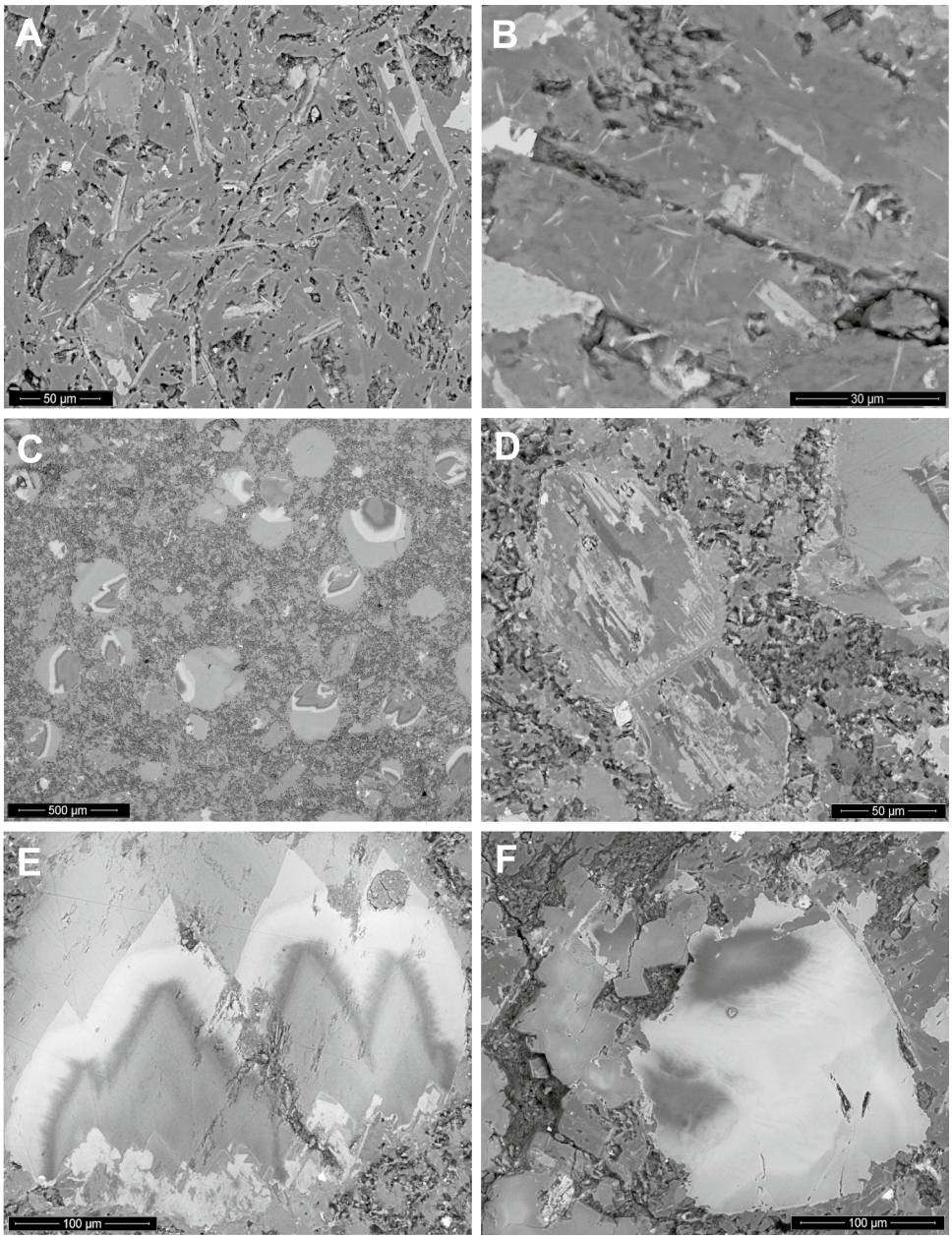

Fig. 4 FESEM-BSE images documenting the composition of clasts of altered basic volcanic rock. **a** matrix with prevailing buddingtonite feldspar, **b** detail of the previous view illustrating the feldspar inhomogeneity, **c** carbonatized part of the clast rim with abundant carbonate-filled amygdales, **d** pseudomorph after olivine, dolomite prevails over quartz and siderite, **e**, **f** transitions between magnesite (darker) and siderite (lighter) in amygdales. Compositional trend in **e** is: Fe-rich magnesite – magnesite (dark zone) – siderite to Mg-rich siderite – dolomite

protodolomite sensu Fang and Xu (2019) are present. In addition to the dolomitic phases (a total of about 80 vol%), the concretions also contain an admixture of quartz, calcite, and muscovite. In FESEM-BSE it is possible to observe that dolomitic carbonate concretions are very fine-grained. Individual dolomite hypidiomorphic grains have a size of up to 5 µm. Unambiguous zoning cannot be observed, but a certain inhomogeneity in BSE is evident. In addition to the dolomitic phase, an admixture of a clastic component (quartz, plagioclase, muscovite), euhedral grains and framboids of pyrite, and cross-sections of foraminifera with a preserved calcite shell are visible.

Discussion

Several modes of buddingtonite occurrences were described worldwide. They include 1) epithermal systems including recent hot-springs, where it could form as a primary mineral (Krohn et al. 1993) or replace older feldspars (Wu et al. 2004; Orberger et al. 2005; Pampeyan 2010; Franz et al. 2017), 2) diagenetic alteration of volcaniclastic rocks deposited in clayey marine sediments rich in organic matter (oil shales), where it originates from volcanic glass or its alteration products, such as montmorillonite or zeolites (Gulbrandsen 1974) or K-feldspars (Loughnan et al. 1983; Oh et al. 1993), 3) coarse-grained sediments associated

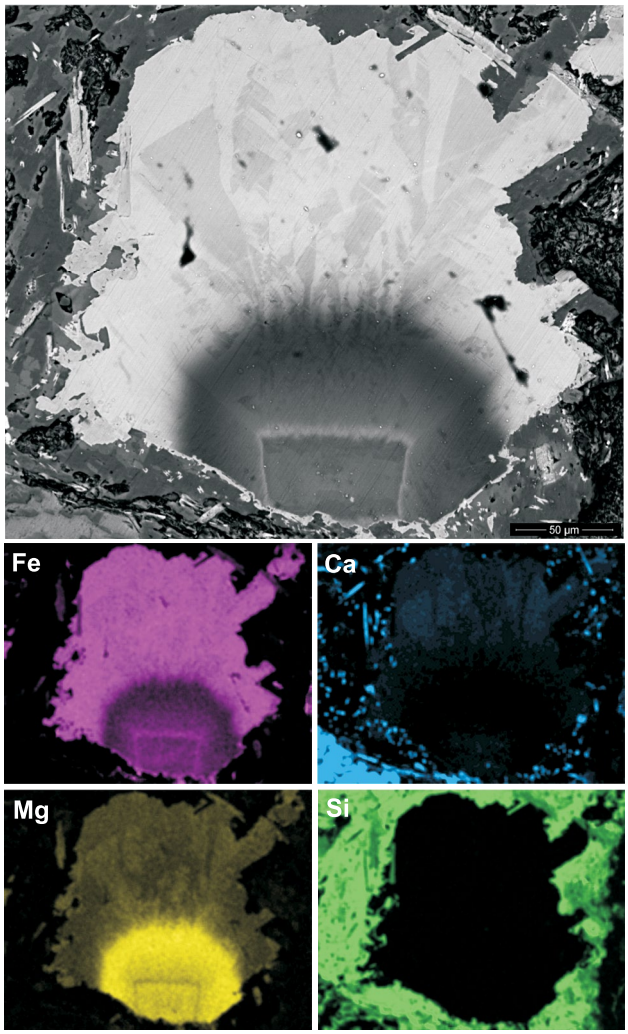

Fig. 5 BSE image and selected element distribution maps from the FESEM-EDS mode. Magnesite-siderite filling of amygdale in altered clast of basic volcanite show magnesite (core) transition to siderite (rim). Silicate rim contains prismatic apatites (see Ca-distribution)

with organic carbon-rich sedimentary sequences, where it replaces K-feldspar in the zone of methanogenesis in an early diagenetic phase (Ramseyer et al. 1993), 4) clay partings in high-sulfur coals, where buddingtonite originate in NH_4^+ substitution for K^+ and in lesser amount also for Na^+ in K-feldspars (Dai et al. 2018).

Based on the appearance of the investigated feldspar aggregates, it is possible to assume that the primary matrix of the studied clasts of basic volcanite was probably formed by feldspar group mineral of feldspathoid, probably with a considerable admixture of glass, which later underwent strong multi-phase alteration recorded in associated minerals. Considering the mode of origin, it is closest to the second point of the previous paragraph.

From the given data, we can anticipate that the geological story linked to buddingtonite origin at the locality begins with the basic volcanism during the Lower Cretaceous. The first phase of alteration processes was connected to olivine phenocrysts after their magmatic crystallization. From the presence of accessory pentlandite and millerite in the olivine pseudomorphs we can say that it was done at low oxygen and higher sulfur fugacity, with presence of water (Filippidis 1982, 1991). The structural features of the clasts, i.e. the distribution of amygdaloid cavities and the crystallinity of the matrix, suggests that rapid rock cooling occurred immediately after the magmatic eruption and they are, in fact, volcanic bombs with a partially glassy surface.

Then, volcanic bombs were incorporated as an exotic clasts into the marine clay sediment. According to the number of papers (e.g., Hall and Fisher 1987; Krása and Matzka 2007; Herrero-Bervera et al. 2011), the alteration of Ti–rich magnetite into the anatase and other breakdown product probably happened after the emplacement, during the ocean-floor metamorphosis within the seafloor. In both possible cases of the sediment age, it was rich in organic matter. For the claystones of the Hradiště Formation, C_{org} varies between 0.55 and 1.95 wt%, with kerogen type II-III and maximum temperatures 80–120 °C, locally up to 220 °C (Menčík et al. 1983; Kubicová and Skupien 2011). During the early diagenesis, we can note the formation of dolomite concretions in the nearby sediment. The origin of CO_2 is linked with the early burial, since the carbon dioxide is a product of direct oxidation of organic matter in sediment (e.g., Mazzullo 2000; Arndt et al. 2013). At this moment the remaining parts of the olivine phenocrysts underwent alteration to mostly dolomitic carbonate, which is the reaction driven mostly by the partial pressure of CO_2 (Li et al. 2019), supported by presence of sodium salts from the seawater (Wang et al. 2019). The excess of magnesium also produced carbonate fillings of amygdales, which show the transition from the oldest Mg-rich via Ca-Mg ones to the youngest Fe-rich. This evolution reflects the restricted access to pure-Mg solutions after the olivine total consumption during its alteration.

With even deeper sediment burial, we can expect entering the oil window (Picha et al. 2006; Kubicová and Skupien 2011). During the catagenesis, nitrogen compounds present in kerogen (e.g., Robinson 1976) partially break down and release ammonium ions (Williams and Ferrell 1991; Williams et al. 1992). Finally, the buddingtonite feldspar was formed by alteration, i.e. ion substitution from feldspar. Since the NH_4^+ ions in the nine fold coordinated A site of the buddingtonite (Harlov et al. 2001) have ionic radius 1.70 Å (Sidey 2016), they can easily replace K^+ ions (ionic radius 1.69 Å) or less preferably Na^+ (1.38 Å) and Ca^{2+} ions (1.32 Å) – see Shannon (1976). Other option would be direct crystallization from the the glass phase, but there is a strong chance of its smectitization in the earlier processes. The youngest mineralization stage is connected with the kaolinite aggregates filling the irregular polygonal spaces in basic rock clasts.

The origin of basic volcanic clasts in the paraconglomerates of the Subsilesian Unit remains a complex and largely

Table 3 Chemical composition and calculated mineral formulae of carbonates from the altered clast of basic volcanite

	Fe-rich magnesite				Mg-rich siderite		Mg-Ca-rich siderite			Calcite	Ca-rich dolomite
Major oxides (wt%)											
CaO	0.38	0.28	0.38	0.88	0.82	1.81	7.91	6.58	6.70	52.88	32.50
MgO	33.16	26.16	38.94	37.43	9.30	9.81	14.08	11.05	10.88	0.35	11.56
FeO	19.41	29.54	12.98	14.37	47.47	45.63	33.33	39.02	39.76	0.82	8.97
MnO	0.23	0.29	0.17	0.24	0.39	0.39	0.52	0.49	0.48	0.09	0.30
CO_2*	48.58	47.11	50.88	50.56	40.18	40.38	42.38	41.47	41.89	42.43	43.81
SiO_2	1.64	0.12	0.06	0.04	0.08	0.03	0.10	0.06	0.04	0.04	0.05
K_2O	0.16	0.04	bdl	bdl	0.01	bdl	0.02	0.01	bdl	0.02	0.01
CoO	bdl	bdl	bdl	bdl	0.07	0.07	0.07	bdl	0.06	bdl	bdl
ZnO	bdl	bdl	bdl	bdl	bdl	bdl	bdl	bdl	0.12	bdl	bdl
total	101.75	103.37	103.35	103.48	98.17	98.03	98.21	98.61	99.72	96.56	97.14
Calculated mineral formulae (apfu)*											
Ca^{2+}	0.006	0.005	0.006	0.014	0.016	0.035	0.146	0.124	0.125	0.977	0.582
Mg^{2+}	0.733	0.606	0.835	0.808	0.252	0.265	0.362	0.291	0.283	0.009	0.288
Fe^{2+}	0.241	0.384	0.156	0.174	0.723	0.692	0.481	0.576	0.581	0.012	0.125
Mn^{2+}	0.003	0.004	0.002	0.003	0.006	0.006	0.008	0.007	0.007	0.001	0.004
CO_3^{2-}	0.983	0.998	1.000	1.000	1.000	1.000	0.999	0.999	1.000	1.000	0.999
Si^{4+}	0.049	0.004	0.002	0.001	0.003	0.001	0.003	0.002	0.001	0.001	0.002
K^+	0.002	-	-	-	-	-	-	-	-	-	-
Co^{2+}	-	-	-	-	0.001	0.001	0.001	-	0.001	-	-
Zn^{2+}	-	-	-	-	-	-	-	-	0.002	-	-

bdl below detection limit

*CO_2 concentrations and mineral formulae were calculated assuming a total of 1.000 divalent cations per formula unit

unanswered question. Eliáš (1998) mentioned an occurrence of clasts of basic igneous rocks without providing further details. It cannot be excluded that these basic igneous rocks belong to the Teschenite Association Rocks–TAR (e.g., Šmíd 1978; Menčík et al. 1983). Based on mineral paragenesis (pseudomorphs after idiomorphic olivines and

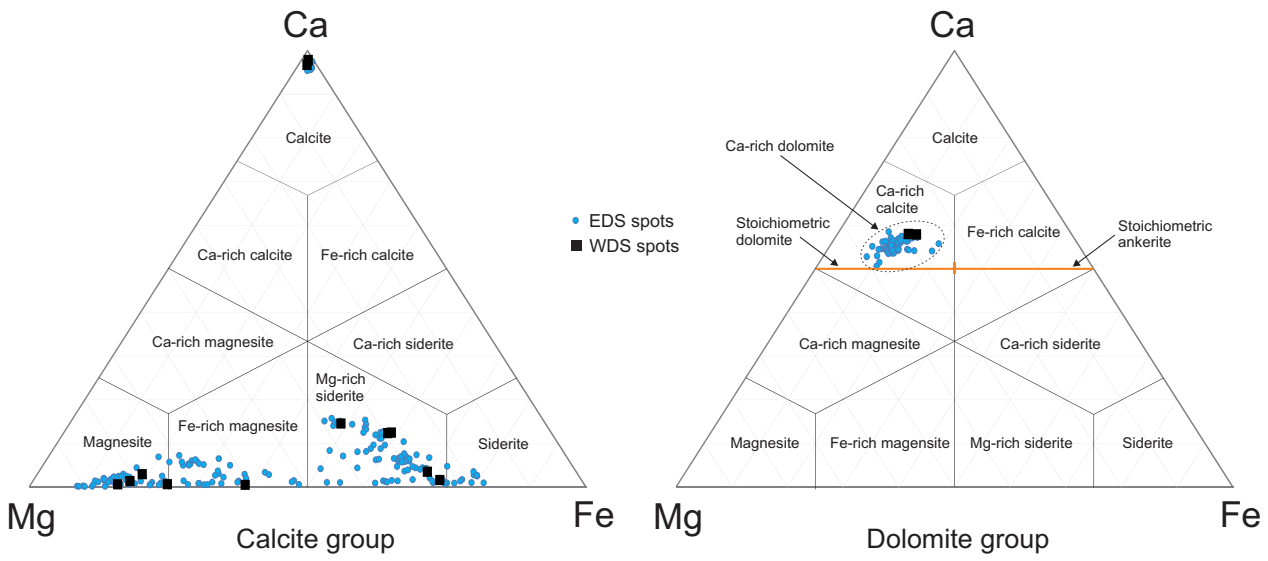

Fig. 6 Ternary plot of Trdlička and Hoffman (1975) showing the composition of carbonates (mol%) of the studied altered clasts of basic volcanite. Analyses projected in the Ca-rich calcite field are in fact Ca-rich dolomites (excess of Ca in the M2-site)

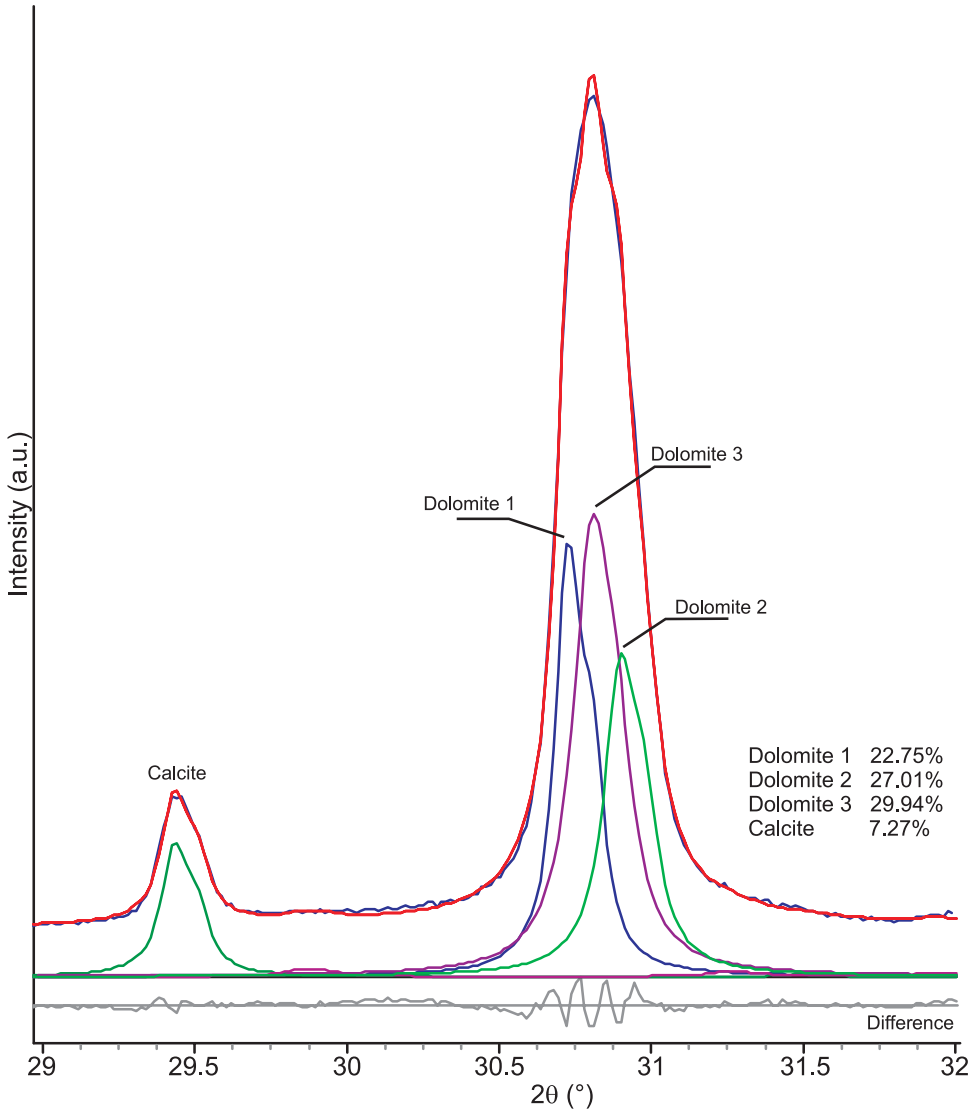

Fig. 7 Decomposition of the diffraction line (104), obtained using Cu-Kα radiation, of the dolomitic phase in carbonate concretions into three components. Unit-cell parameters are: dolomite-1 a = 4.8281(2), c = 16.1593(7) Å; dolomite-2 a = 4.8119(2), c = 16.0396(11) Å; dolomite-3 a = 4.8200(2), c = 16.0996(10) Å. Note that calcite diffraction line is homogenous

accessories), after subtracting all alterations, the studied clasts could correspond to some monchiquites, or their transitions to picrites. Carpathian occurrences of the TAR are of Early Cretaceous age and occur mainly in the Hradiště Formation of the Silesian Unit (e.g. Brunarska and Anckiewicz 2019). In such case, the mechanism of transport of volcanic clasts from the Early Cretaceous of the Silesian Basin to the Late Cretaceous part of the Subsilesian Basin would be unclear. It would require, among others, erosion and transport in the period between Aptian/Albian and Maastrichtian, which is not expected according to contemporary models of the Carpathian orogen evolution. Other Mesozoic sources of basic volcanic rocks are even much more distant–Tatricum, Križná and Choč nappes (e,g., Hovorka and Spišiak 1988, 1993).

However, it is worthy of note that the strata at the buddingtonite locality has several features characteristic for the Silesian Unit rather than the Subsilesian Unit, which would make the investigated volcanic clast autochtonous. They are: (i) Sandstone-conglomerate sequence consists of of Istebna-type sandstone and conglomerate. (ii) Pebbly mudstone enclose large clasts of the Štramberk-type limestone that are according to some authors (Eliáš 1998) uncommon in the Czech part of the Subsilesian Unit. Newly published data from the neighboring Poland (Hoffmann et al. 2021) contradict this statement, but one should keep in mind that the Subsilesian Unit definition differ somehow in both countries. (iii) Dark-gray mudstones from the outcrop higher upstream contained agglutinated foraminifer assemblage dominated by *Praesphaerammina gerochi* (H.) characteristic for the Danian of the Silesian Unit. (iv) Extensive outcrop downstream the section belongs to the Krosno Formation of the Silesian Unit. Stratigraphical equivalent in the Subsilesian Unit is lithofacially different Ženklava Formation (compare Bubík et al. 2016).

Anyhow, the microfossil assemblages received from mudstones of the studied buddingtonite locality is typical for the Frýdek Formation and we consider it as a part of the Subsilesian Unit tentatively. It cannot be excluded that some tectonic slices exposed in Ostravice River bed belong to the Silesian Unit, but this will be subject of further investigation.

Conclusions

The mineralogical composition of clasts of basic volcanic rocks from the Frýdek Formation of the Subsilesian Unit was studied. The clasts, originally volcanic bombs, were found in the paraconglomerate layer within the sandstone-conglomerate sequence that forms clastic body within the pebbly mudstones. The structural features, i.e. the distribution of amygdaloid cavities and the crystallinity of the matrix, suggesting that the clasts may have been volcanic bombs with a partially glassy surface. Clasts are extremely strongly altered, carbonatized, and transformed into clay minerals. Buddingtonite feldspar with about 50–60 mol% of the buddingtonite component is part of the rock matrix. Amygdales contain grains and complex crystals formed by transitions between magnesite and siderite. The clasts alteration was probably polyphase, but the alteration in the diagenetic and katagenetic conditions during the formation of carbonate concretions had a decisive influence on the final composition. Buddingtonite feldspar was probably formed by alteration, i.e. ion exchange from plagioclase or the glass phase in an environment with a high content of ammonium ions, released from the organic matter decomposition.

Concerning its geological setting, the described occurrence presents a transition between buddingtonite formed in marine organic-rich shales (Gulbrandsen 1974; Loughnan et al. 1983; Oh et al. 1993) and buddingtonite formed by direct alteration of volcanic rocks (Erd et al. 1964; Pampeyan 2010). This report gives evidence for the first buddingtonite occurrence in the Carpathian Mountains (Szakáll et al. 2002) and second in Europe after Volyn pegmatite II in Ukraine (Franz et al. 2017).

Carbonate concretions in the proximity of altered volcanic clasts are dolomitic. For the area of Podbeskydí and the Moravian-Silesian Beskydy Mts., this is somewhat atypical, since diagenetic carbonate concretions composed of variable degree of substituted siderite predominate here (Roth and Matějka 1953; Buriánek et al. 2011; Matýsek and Jirásek 2021). Until now, dolomitic concretions have been observed only in the Silesian Unit, in the Istebná Formation, which is stratigraphic equivalent to the Frýdek Formation (unpublished data D. Matýsek). From the Polish part of the Outer Carpathians, it is mentioned, for example, by Bojanowski (2014).

Supplementary Information The online version contains supplementary material available at https://doi.org/10.1007/s00710-022-00794-y.

Acknowledgements Constructive comments by two anonymous reviewers and handling editor Nikita V. Chukanov are gratefully acknowledged. The present study was supported by Grant Agency of the Czech Republic projects 19-07516S and 20-04505S. We have used equipment financed by the Ministry of Youth, Education and Sports of Czech Republic, grant LO1406.

References

Angel RJ, Ross NL, Zhao J, Sochalski-Kolbus L, Kruger H, Schmidt BC (2013) Structural controls on the anisotropy of tetrahedral frameworks: the example of monoclinic feldspars. Eur J Mineral 25:597–614

Arndt S, Jørgensen BB, LaRowe DE, Middelburg JJ, Pancost RD, Regnier P (2013) Quantifying the degradation of organic matter in marine sediments: a review and synthesis. Earth-Sci Rev 123:53–86

Bojanowski MJ (2014) Authigenic dolomites in the Eocene-Oligocene organic carbon-rich shales from the Polish Outer Carpathians: Evidence of past gas production and possible gas hydrate formation in the Silesian basin. Mar Petrol Geol 51:117–135

Brunarska I, Anckiewicz R (2019) Geochronology and Sr–Nd–Hf isotope constraints on the petrogenesis of teschenites from the type-locality in the Outer Western Carpathians. Geol Carpath 70:222–240

Bubík M, Franců J, Gilíková H, Otava J, Švábenická L (2016) Upper Cretaceous to Lower Miocene of the Subsilesian Unit (Western Carpathians, Czech Republic): stratotypes of formations revised. Geol Carpath 67:239–256

Buriánek D, Bubík M, Krejčí O (2011) Carbonate concretions of the Moravsko-Slezské Beskydy Mountains (Czech Republic). Geol Výzk Mor Slez 18:13–18 (in Czech with English abstract)

Dai S, Xie P, French D, Ward CR, Graham IT, Yan X, Guo W (2018) The occurrence of buddingtonite in super-high-organic-sulphur coals from the Yishan Coalfield, Guangxi, southern China. Int J Coal Geol 195:347–361

Eliáš M (1998) Sedimentology of the Subsilesian Unit. Czech Geological Survey, Praha, 48 pp (in Czech with English abstract)

Erd RC, White DE, Fahey JJ, Lee DE (1964) Buddingtonite, an ammonium feldspar with zeolitic water. Am Mineral 49:831–850

Fang Y, Xu H (2019) A new approach to quantify the ordering state of protodolomite using XRD, TEM, and Z-contrast imaging. J Sediment Res 89:537–551

Filippidis A (1982) Experimental study of the serpentinization of Mg-Fe-Ni olivine in the presence of sulfur. Can Mineral 20:567–574

Filippidis A (1991) Further comments on the opaque mineral assemblages in ultramafic rocks – an experimental study. Ofioliti 16:1–6

Franz G, Khomenko V, Vishnyevskyy A, Wirth R, Struck U, Nissen J, Gernert U, Rocholl A (2017) Biologically mediated crystallization of buddingtonite in the Paleoproterozoic: Organic-igneous interactions from the Volyn pegmatite, Ukraine. Am Mineral 102:2119–2135

Gulbrandsen RA (1974) Buddingtonite, ammonium feldspar, in the Phosphoria Formation, southeastern Idaho. J Res USGS 2:693–697

Hall JM, Fisher BE (1987) The characteristics and significance of secondary magnetite in a profile through the dike component of the Troodos, Cyprus, ophiolite. Can J Earth Sci 24:2141–2159

Harlov DE, Andrut M, Pöter B (2001) Characterization of buddingtonite (NH_4)[$AlSi_3O_8$] and ND_4- buddingtonite (ND_4)[$AlSi_3O_8$] using IR spectroscopy and Rietveld refinement of XRD spectra. Phys Chem Miner 28:188–198

Herrero-Bervera E, Acton G, Krása D, Rodriguez S, Dekkers MJ (2011) Rock magnetic characterization through an intact sequence

of oceanic crust, IODP hole 1256D. In: Petrovský E, Ivers D, Harinarayana T, Herrero-Bervera E (eds) Earth's magnetic interior. IAGA Special Sopron Book Series, Springer, Dordrecht, pp 153-168

Hoffmann M, Kołodziej B, Kowal-Kasparzyk J (2021) A lost carbonate platform deciphered from clasts embedded in flysch: Štramberk-type limestones, Polish Outer Carpathians. Ann Soc Geol Pol 91:203–251

Hovorka D, Spišiak J (1988) Mesozoic volcanism of the Western Carpathians. Veda, Bratislava, 263 pp (in Slovak with English and Russian summary)

Hovorka D, Spišiak J (1993) Mesozoic volcanic activity of the Western Carpathian segment of the Tethyan Belt: Diversities in space and time. Jahrb Geol B-A 136:769–782

Kimball MR, Megaw HD (1974) Interim report on the crystal structure of buddingtonite. In: MacKenzie WS, Zussman J (eds) Feldspars. Manchester, Manchester Press, Proc NATO ASI on Feldspars, pp 81–86

Krása D, Matzka J (2007) Inversion of titanomaghemite in oceanic balat during heationg. Phys Earth Planet in 160:169–179

Krohn MD, Kendall C, Evans JR, Fries TL (1993) Relations of ammonium at several hydrothermal systems in the western U.S. J Volcanol Geoth Res 56:401–413

Kubicová P, Skupien P (2011) Organic matter in the Cretaceous deposits of the Outer Western Carpathians and their source potential for oil and gas. Geosci Res Rep 44:26–30 (in Czech with English summary)

Li J, Jacobs AD, Hitch M (2019) Direct aqueous carbonation on olivine at a CO_2 partial pressure of 6.5 MPa. Energy 173:902–910

Loughnan FC, Roberts FI, Lindner AW (1983) Buddingtonite (NH_4-feldspar) in the Condor Oilshale Deposits, Queensland, Australia. Mineral Mag 47:327–334

Matýsek D, Jirásek J (2021) Manganese-rich carbonate and phosphate concretions from the Subsilesian Unit of the Outer Western Carpathians (Czech Republic): Composition and unique selenium weathering products. Geol Carpath 72:155–169

Mazzullo SJ (2000) Organogenic dolomitization in peritidal to deep-sea sediments. J Sed Res 70:10–23

Menčík E, Adamová M, Dvořák J, Dudek A, Jetel J, Jurková A, Hanzlíková E, Houša V, Peslová H, Rybářová L, Šmíd B, Šebesta J, Tyráček J, Vašíček Z (1983) Geology of the Moravskoslezské Beskydy Mts. and the Podbeskydská pahorkatina Upland. Academia, Praha, 307 pp (in Czech with English summary)

Merlet C (1994) An accurate computer correction program for quantitative electron probe microanalysis. Microchim Acta 114–115:363–376

Mookherjee M, Redfern SAT, Swainson I, Harlov DE (2004) Low-temperature behaviour of ammonium ion in buddingtonite [$N(D/H)_4AlSi_3O_8$] from neutron powder diffraction. Phys Chem Miner 31:643–649

Oh MS, Foster KG, Alcaraz A, Crawdord RW, Taylor RW, Coburn TT (1993) Thermal decomposition of buddingtonite in oil shales. Fuel 72:517–523

Orberger B, Gallien J-P, Pinti DL, Fialin M, Daudin L, Gröcke DR, Pasava J (2005) Nitrogen and carbon partitioning in diagenetic and hydrothermal minerals from Paleozoic Black Shales, (Selwyn Basin, Yukon Territories, Canada). Chem Geol 218:249–264

Pampeyan EI (2010) Buddingtonite in Menlo Park, California. U.S. Geological Survey Open-File Report 2010–1053:1–10

Picha, FJ, Stráník Z, Krejčí O (2006) Geology and hydrocarbon resources of the Outer Western Carpathians and their foreland, Czech Republic. In: Golonka J, Picha J (eds) The Carpathians and their foreland: geology and hydrocarbon resources. AAPG Memoir. Tulsa. pp 84:49–175

Pöter B (2003) Experimentally determined K-NH_4 partitioning between feldspars, muscovites and aqueous chloride solutions. Ph.D. thesis, Technische Universität Berlin

Pöter B, Gottschalk M, Heinrich W (2007) Crystal-chemistry of synthetic K-feldspar–buddingtonite and muscovite–tobelite solid solutions. Am Mineral 92:151–165

Ramseyer K, Diamond LW, Boles JR (1993) Authigenic K-NH_4-feldspar in sandstones: a fingerprint of the diagenesis of organic matter. J Sediment Petrol 63:1092–1099

Robinson WE (1976) Origin and characteristics of Green River oil shale. In: Yen TF, Chilingarian GV (eds) Oil shale. Dev Petroleum Sci 5. Amsterdam – Oxford – New York, Elsevier, pp 61–79

Roth Z, Matějka A (1953) The pelosiderites of the Moravosilesian Beskydy. Nakladatelství Československé akademie věd, Praha, 111 pp (in Czech with English and Russian abstracts)

Shannon RD (1976) Revised effective ionic radii and systematic studies of interatomic distances in halides and chalcogenides. Acta Cryst A32:751–767

Sidey V (2016) On the effective ionic radii for ammonium. Acta Cryst B72:626–633

Szakáll S, Udubaşa G, Ďuďa R, Kvasnytsya V, Koszonska E, Novák M (2002) Minerals of the Carpathians. Granit, Prague, 479 pp

Šmíd B (1978) Výzkum vyvřelých hornin těšínitové asociace. Rigorous thesis, Ústřední ústav geologický Praha (in Czech)

Trdlička Z, Hoffman V (1975) Untersuchungen der chemischen Zusammensetzung der Gangkarbonate von Kutná Hora (ČSSR). Freiberg Forsch C 321:29–81 (in German)

Venari CE, O`Bonnon EE, Williams Q (2017) The ammonium ion in a silicate under compression: infrared spectroscopy and powder X-ray diffraction of $NH_4AlSi_3O_8$ buddingtonite to 30 GPa. Phys Chem Miner 44:149–161

Voncken JHL, Konings RJM, Jansen JBH, Woensdreght CF (1988) Hydrothermally grown buddingtonite, an anhydrous ammonium feldspar ($NH_4AlSi_3O_8$). Phys Chem Miner 15:323–328

Voncken JHL, van Roermund HLM, van der Eerden AMJ, Jansen JBH, Erd RC (1993) Holotype buddingtonite: an ammonium feldspar without zeolitic H_2O. Am Mineral 78:204–209

Wang F, Dreisinger D, Jarvis M, Hitchins T (2019) Kinetics and mechanism of mineral corbonation of olivine for CO_2 sequestration. Miner Eng 131:185–197

Williams LB, Ferrell RE (1991) Ammonium substitution in illite during maturation of organic matter. Clay Clay Miner 39:400–408

Williams LB, Wilcoxon BR, Ferrell RE, Sassen (1992) Diagenesis of ammonium during hydrocarbon maturation and migration, Wilcox Group, Louisiana, U.S.A. Appl Geochem 7:123–134

Wu J, Huang Z, Luo T (2004) Contents of fixed-ammonium (NH_4^+) in lamprophyres in the Thenyuan Gold Orefield, Yunnan Province, China: implications for its characteristics of the source region. Chinese J Geochem 23:186–190